

ESTIMATING ABOVEGROUND BIOMASS OF  
PASTURE ENVIRONMENTS USING  
STRUCTURE FROM MOTION

by

David Szpakowski, BS

A thesis submitted to the Graduate Council of  
Texas State University in partial fulfillment  
of the requirements for the degree of  
Master of Science  
with a Major in Geography  
August 2016

Committee Members:

Jennifer Jensen

Jason Julian

Nathan Currit

**COPYRIGHT**

by

David Szpakowski

2016

## **FAIR USE AND AUTHOR'S PERMISSION STATEMENT**

### **Fair Use**

This work is protected by the Copyright Laws of the United States (Public Law 94-553, section 107). Consistent with fair use as defined in the Copyright Laws, brief quotations from this material are allowed with proper acknowledgment. Use of this material for financial gain without the author's express written permission is not allowed.

### **Duplication Permission**

As the copyright holder of this work I, David Szpakowski, authorize duplication of this work, in whole or in part, for educational or scholarly purposes only.

## **ACKNOWLEDGEMENTS**

First and foremost, I would like to acknowledge my advisor Dr. Jennifer Jensen for all of the advice, guidance, and mentoring over the past two years. Her support truly pushed me to become a better researcher every step of the way, for which I cannot thank her enough.

I would like to thank my committee members, Drs. Jason Julian and Nathan Currit, whose edits, comments, and suggestions strengthened this research.

I would also like to thank Dr. Susan Schwinning, who generously allowed me to use her lab equipment to conduct my research.

A special thanks for my close friends in and out of the department who would listen to me ramble on about my research, and encourage me every step of the way.

Finally, I would like to acknowledge all the support I received from my family, particularly my parents, Jim and Sally Szpakowski, who always believed in me and provided me all the necessary support to achieve my dreams.

## TABLE OF CONTENTS

	Page
ACKNOWLEDGEMENTS .....	iv
LIST OF TABLES .....	vii
LIST OF FIGURES .....	viii
LIST OF ABBREVIATIONS.....	vix
CHAPTER	
I. INTRODUCTION .....	1
1.1 Background.....	1
1.2 Problem Statement.....	3
1.3 Research Objectives.....	4
1.4 Justification.....	4
II. LITERATURE REVIEW.....	6
2.1 Pastures and aboveground biomass .....	6
2.2 Spectral-based measurements of AGB .....	7
2.3 Lidar-based measurement of AGB .....	9
2.4 Structure from Motion as an alternative to lidar data .....	13
III. MATERIALS AND METHODS.....	16
3.1 Study area.....	16
3.2 Field Data.....	18
3.3 Image Acquisition, Processing, and Point Cloud Generation.....	20
3.4 SfM metric calculations .....	23
3.5 Statistical Analysis.....	24
IV. RESULTS .....	26
4.1 AGB Field Measurements.....	26
4.2 Results of the SfM and Lidar Point Clouds .....	29

4.3 Statistical Relationship between SfM Variables and Field Measured AGB.....	32
V. DISCUSSION .....	35
5.1 SfM prediction of AGB .....	35
5.2 SfM and Lidar Inconsistencies.....	36
5.3 Causes of Uncertainty and Limitations to the SfM Method .....	38
5.4 Potential Improvements .....	42
VI. CONCLUSION.....	45
LITERATURE CITED .....	46

## LIST OF TABLES

<b>Table</b>	<b>Page</b>
1. Summary of Metrics .....	24
2. Above-ground biomass (AGB) weights by plot .....	27
3. Descriptive statistics of AGB in field-measured plots, excluding outliers .....	29
4. SfM and lidar data measurements .....	29
5. Descriptive statistics of the SfM derived metrics .....	32
6. Goodness-of-fit statistics for individual metrics .....	33
7. Summary of model statistics .....	34

## LIST OF FIGURES

<b>Figure</b>	<b>Page</b>
1. Study Area .....	17
2. Location of plots used for collecting AGB .....	19
3. Example of a flight path with GCP locations .....	21
4. Distribution of AGB weights .....	28
5. Distribution of the number of points per plot .....	30
6. Birds-eye view of the study area's SfM point cloud.....	31
7. Oblique view of the study area's SfM point cloud .....	31
8. Close-up view of the SfM point cloud on plots 1-3.....	32
9. Two SfM covariate multiple regression model of actual versus predicted AGB .....	34
10. Example of a warped edge in the SfM point cloud.....	41
11. Example of two plots affected by warping along the edges .....	41

## LIST OF ABBREVIATIONS

<b>Abbreviation</b>	<b>Description</b>
AGB	Above-ground Biomass
BDR	Normalized Band Depth Ratio
BGB	Below-ground Biomass
BNA	Band Depth Normalized to Band Area
CAPCOG	Capital Area Council of Governments
CHP	Canopy Height Profiles
CV	Coefficient of Variation
DEM	Digital Elevation Model
DSM	Digital Surface Model
EVI	Enhanced Vegetation Index
FS	Front Slope Angle
GCP	Ground Control Point
GPS	Global Positioning Systems
$H_{max}$	Maximum Height
$H_{mean}$	Height Mean
$H_{median}$	Median Height
$H_{min}$	Minimum Height
$H_{SD}$	Standard Deviation of Height
$H_{10}$	10 <sup>th</sup> Percentile Height
$H_{90}$	90 <sup>th</sup> Percentile Height
HOME	Height of Mean Energy
$H_p$	Percentile Height
HTMR	Height/Mean Ratio
IMU	Inertial Measurement Unit
LAI	Leaf Area Index
LAS	Log ASCII Standard
Lidar	Light Detection and Ranging
LPI	Laser Penetration Metric
MCH	Mean Canopy Height
MSR	Modified Simple Ratio
MTCI	MERIS Terrestrial Chlorophyll Index
NBDI	Normalized Band Depth Index
NDMI	Normalized Difference Moisture Index
NDVI	Normalized Difference Vegetation Index
NDWI	Normalized Difference Water Index
NIR	Near-infrared

NP	Number of Peaks
PC <sub>2.5</sub>	Percent Cover above 2.5 cm
PC <sub>3.5</sub>	Percent Cover above 3.5 cm
PC <sub>5</sub>	Percent Cover above 5 cm
PRESS	Predicted Residual Error Sum of Squares
REIP	Red Edge Inflection Point
ROUGH	Roughness of Outermost Canopy
RWE	Return Waveform Energy
SAVI	Satellite-based Augmentation System
SBAS	Soil Adjusted Vegetation Index
SfM	Structure from Motion
SSV	Sum of Squared Errors
SVR	Shortwave-infrared/Visual Ratio
TCG	Tasseled Cap Transformation's Greenness
TCW	Tasseled Cap Transformation's Wetness
TLS	Terrestrial Laser Scanning
TSAVI	Transformed Soil Adjusted Vegetation Index
UAV	Unmanned Ariel Vehicle
V	Variance
VDR	Vertical Distribution Ratio
VI	Vegetation Index
WD	Waveform Distance

# I. INTRODUCTION

## 1.1 Background

Pastures are areas of land covered with grass and other low lying vegetation which is suitable for animal grazing. As such, pastures play a critical role in the raising of livestock and environmental management (Jin et al. 2014; Zhao et al. 2014). Being able to obtain accurate estimations of the above-ground biomass (AGB) within a pasture is important when it comes to designing a management plan for the pasture and surrounding ecosystem. AGB is defined as the total living biomass above the soil, including all parts of the plant that exist per unit area.

Many remote sensing techniques have been developed to estimate AGB for different environments, including pastures (Drake et al. 2003; Gao et al. 2012; He 2013; Barrachina et al. 2014; Raval et al. 2014; Zhao et al. 2014; Kaasalainen et al. 2015). With the development of satellite technology and more advanced aerial photography, remote sensing methods and estimates of AGB have become increasingly complex and more accurate. Spectral analyses and vegetation indices were initially used and further refined as specific characterizations of plant health, density, and height were required for vegetation and ecosystem process models. At present, satellite and aerial imagery are considered acceptable data sets for AGB estimates.

The introduction of airborne Light Detection and Ranging (lidar) technology in the late 1990s provided a new method for collecting and analyzing spatial data. Unlike traditional optical imagery, lidar produces a 3D point cloud derived from an active near-infrared sensor, which results in increased accuracy for vegetation height modeling. As AGB tends to increase with vegetation height, the ability to produce a 3D model of

vegetation structure and height will allow for biomass estimates from lidar using allometric equations. Because of this lidar is now seen as one of the most accurate means of measuring AGB (Lefsky et al. 2002; Cao et al. 2014), albeit one of the most costly.

Structure from Motion (SfM) and subsequent dense point matching, also referred to as image-based point clouds, is a relatively new technology that is rapidly becoming a cost effective alternative lidar datasets (Westoby et al. 2012; White et al. 2013). Applications of SfM point clouds are numerous, including the creation of high resolution digital elevation models (DEMs) (Fonstad et al., 2013), analyzing and monitoring soil erosion (Kaiser et al 2014), and creating 3D models of urban features (Snavely et al. 2006; Richter et al. 2013). This new technology is based on traditional photogrammetric techniques which allow multiple images of an object, or area, to be combined via algorithms. The algorithms are based on linear algebra and produce a 3D point cloud representing features of interest at a relatively low cost compared to lidar data acquisitions (Westoby 2012; White et al. 2013). The imagery is usually obtained via the use of inexpensive digital cameras which are either hand held or mounted to an unmanned aerial vehicle (UAV). When mounted to a UAV, the camera will fly a predetermined flight path around the object of interest while obtaining imagery for subsequent image mosaicking and dense point matching to produce a 3D point cloud. Applications of this technology have already proven to be comparable to lidar, but as it is a new technology there are still uncertainties associated with its capabilities and limitations (Leberl et al. 2010; White et al. 2013).

As SfM point clouds offer a cost effective alternative to lidar (Westoby et al. 2012; White et al. 2013) it is now important to assess whether this technology can be used to

estimate AGB using methods originally employed for lidar. As both lidar and SfM produce point clouds in order to perform analysis, and as these point clouds have proven to be very close to one another in terms of accuracy (Leberl et al. 2010; White et al. 2013), applying previously used lidar methods to SfM models should be possible. While numerous studies have been completed on the estimation of above-ground biomass using lidar (Drake et al. 2003; He 2013; Kaasalainen et al. 2015; Cao et al 2014; Lefsky et al. 2002) there are far fewer studies which attempt to test this ability through the use of Structure from Motion.

The objective of this study is to determine if previously published methods for estimating AGB using lidar based point clouds can be applied to SfM point clouds. Studies published in the last five years indicate that lidar processing and analysis methods are applicable to SfM point cloud data (Dandois et al. 2010; Westoby et al. 2012; Mancini et al. 2013). Thus, there is a high likelihood that methods developed for lidar-estimated AGB will be applicable for SfM point clouds.

## 1.2 Problem Statement

An application of SfM that has yet to be studied is the utility of SfM point clouds to estimate above-ground biomass in pasture environments. Characterization of AGB is important because of its relation to other estimates such as forage biomass, soil nutrient allocation, fuel accumulation, and other important environmental variables (Lu 2005), many of which can be characterized or monitored using remotely sensed datasets. This study will identify the necessary metrics for estimating AGB of pastures using SfM point clouds, as well as documenting any limitations that arise when using the technology for this purpose. While the lidar techniques were mainly developed for estimating the AGB

of forest environments (Drake et al. 2003; He 2013; Kaasalainen et al. 2015) some of the methods should be applicable to pasture environments as well since lidar and SfM are both 3D point cloud data.

### 1.3 Research Objectives

This study will evaluate whether SfM point clouds can be used to estimate the AGB of a pasture. Specifically, the following research objectives will be addressed:

- Objective 1: Assess the utility of Structure-from-Motion products to estimate AGB of a pasture.
- Objective 2: Document limitations of the SfM method for pasture AGB estimation

### 1.4 Justification

SfM has many key advantages over lidar, including cost, temporal resolution, and a higher average point density. SfM can generate point clouds at a fraction of the cost of lidar due to its use of imagery derived from low-cost cameras. This allows data collection to be performed by aerial vehicles such as UAVs, as opposed to the airplanes and helicopters which are the normal vehicles involved in the collection of lidar data. Because of this the cost of data collection is not only decreased, but the temporal resolution is increased. With UAVs, data collection can happen in much shorter intervals than with planes or helicopters due both to ease of use and cost. This higher temporal resolution allows for more up-to-date data to be used in analyses. Finally, because of how SfM generates point clouds it tends to have a higher point density. While this is not always

desirable, it is in the case of this study because of the need to model vegetation structures at a fine scale. With this higher point density, it should be possible to differentiate grasses and other low-lying vegetation from one another, something lidar derived data would normally have trouble accomplishing.

It is important to find what the technology is currently capable of achieving as well as what current limitations exist when using this technology. As there are already many models and algorithms developed for measuring above-ground biomass with lidar and other remote sensing technologies, it is now prudent to find if these same models are applicable to pastures which are mapped with SfM point clouds. This is especially important as SfM point clouds represent a means of collecting data that is far more affordable, efficient, and reliable for environmental managers than that of most other remote sensing methods.

## II. LITERATURE REVIEW

### 2.1 Pastures and aboveground biomass

The importance of pastures in environmental research is a result of the environmental controls they help maintain. Pastures play a crucial role in agricultural activities such as the raising of livestock, erosion prevention, water conservation, energy exchange, air purification, and biochemical cycles among other important environmental control factors (Jin et al. 2014; Zhao et al. 2014). As a result, the importance of estimating the AGB of pastures rapidly as well as accurately is a significant scientific endeavor for the better management and understanding of modern agricultural and environmental health considerations (Zhao et al. 2014). Pastures represent an important environment that can be better managed as techniques for gathering key environmental data progress. An important attribute of a pasture is the AGB, because from this attribute it is possible to estimate forage biomass, carbon sequestration, fuel accumulation, soil nutrient allocation, and other important environmental variables (Drake et al. 2003; Lu 2005). Once these variables are estimated the ability for environmental managers to create plans for conservation and land use becomes more achievable due to the increase in knowledge about the environmental capacity of pastures under scrutiny.

While originally estimated by *in situ* methods, it has become increasingly common to use remote sensing data to estimate AGB (Gao et al. 2012; Porter et al. 2014; Raval et al. 2014; Zhao et al. 2014). While image analysis originally relied on the use of single-band information for estimation, issues arose from errors in the data which lead to the use of vegetation indexes (VIs) for building estimation models (Zhao 2014). The use of spectral analysis became common place, as well as the development of different

indexes to estimate vegetation health and biomass. These developments led to advances in ecosystem management by natural resource managers.

## 2.2 Spectral-based measurements of AGB

Spectral analysis of above-ground biomass has been a topic of interest for decades and is still an active area of research. Raval et al. (2014) used satellite based estimates of biomass in reclaimed coal mines of Central Appalachia. The study used four different vegetation indexes including: normalized difference vegetation index (NDVI), normalized difference moisture index (NDMI), shortwave-infrared/visual ratio (SVR), and modified simple ratio (MSR). Two band ratios and four band transformations were also used in order to identify which method was best suited for estimating above-ground biomass. These 10 spectral derivative values were then regressed against the in situ biomass measurements for each area of interest. The study found that NDVI and MSR both provided high levels of estimate accuracy while NDMI and SVR performed relatively poorly.

Porter et al. (2014) used a combination of Landsat 5 and 7 imagery as well as crop circle sensors to estimate biomass from pasture land enrolled in the Conservation Reserve Program. The study used regression models constructed from NDVI and various band combinations in order to find which models would demonstrate a statistically significant relationship between measured and modeled estimates. They found that none of the models demonstrated a statistically significant difference between measured and modeled estimates and that the usefulness of red, red-edge, and near-infrared (NIR) spectral regions were most responsive during boot and peak growth stages of vegetation.

In a study performed by Barrachina et al. (2014), Landsat 5 was used in order to estimate AGB in a mountain meadow located in Vall Fosca, Spain. Using multiple linear regression where field-based measurements served as dependent variables and vegetation and wetness indices derived from the Landsat data served as predictor variables. The vegetation and wetness indices selected for the study were NDVI, enhanced vegetation index (EVI), tasseled cap transformation's greenness (TCG), tasseled cap transformation's wetness (TCW), and normalized difference water index (NDWI). The study found that AGB models yielded the best results in midsummer with a mean  $R^2$  of 0.74. Wetness indices were found to be more useful for estimating AGB of meadows and pastures under high canopy cover, while the traditional vegetation indices proved less useful.

Ullah et al. (2012) performed a study which examined the use of MERIS data in estimating grassland biomass. A variety of vegetation indices were used including NDVI, soil adjusted vegetation index (SAVI), transformed soil adjusted vegetation index (TSAVI), red edge inflection point (REIP), and MERIS terrestrial chlorophyll index (MTCI), as well calculating the band depth analysis parameters of normalized band depth ratio (BDR), normalized band depth index (NBDI), and band depth normalized to band area (BNA). The study found that the band depth analysis parameters were better predictors than vegetation indices for AGB, concluding that band depth analysis parameters could be used to monitor grassland conditions on regional scales.

A study performed by Gitelson et al. (2003) attempted to estimate leaf area index (LAI) in maize canopies, located in two large irrigated production fields. The study developed two new approaches to estimate LAI and green leaf biomass, through the use

of the green and red edge portions, as well as the NIR portion. These indices were calculated as follows:  $[(\text{NIR}/\text{Green}) - 1]$  and  $[(\text{NIR}/\text{RedEdge}) - 1]$ . The study found a close relationship between these indices and LAI as well as green leaf biomass, indicating that they may prove useful for estimations of these two attributes while acknowledging that more research into the effectiveness of these indices is necessary.

### 2.3 Lidar-based measurement of AGB

In the late 1990s, lidar began to emerge as a new remote sensing technology with the ability to gather different types of data on an area than was possible with previous technologies. Lidar systems emit pulses of NIR energy toward the surface and these pulses are then reflected back to the sensor. Through the use of global positioning systems (GPS), inertial measurement unit (IMU), and the time lapse for the pulse to return, the exact position of where the pulse was reflected from is determined. This process is repeated with each pulse and the positional information of all the pulses is combined and interpolated to create a 3D point cloud with extremely high positional accuracy.

Lidar is able to characterize structure by producing a 3D point cloud representation of the surface features. The accuracy of lidar-based measurements proved the usefulness of the new technology for environmental management as it could be used to examine height and structure of various elements within an environment. While there are plenty of articles which illustrate lidar's strength in assisting with estimating AGB, there are none (to the best of my knowledge) in which this technique is applied to a pasture specifically.

The use of lidar for AGB estimates is focused primarily in forest environments.

Drake et al. (2003) used lidar to estimate above-ground biomass in closed canopy Neotropical forests located in Panama and Costa Rica. The study used two metrics (canopy height, height of median energy) to estimate above-ground biomass in the two tropical forests. It was found that AGB estimates were significantly different between the two tropical forests, mainly attributed to a drought that existed in one of them during the period of study.

He et al. (2013) used lidar to estimate the AGB of an area of coniferous forest located on Qilian Mountain in western China. The metrics used in this study were mean vegetation height, percentile vegetation height, and canopy cover for the estimation of above-ground biomass. The study found that these metrics gave a relatively accurate predictive model for above-ground biomass.

In the study conducted by Lefsky et al. (2002), lidar was used to estimate AGB of forests in three different biomes. The three study areas were part of the Cascade Range, Oregon (temperate coniferous forest), Smithsonian Environmental Research Center located on the western shore of Chesapeake Bay (temperate deciduous forest), and the Northern Old Black Spruce study area located in north-central Canada (boreal coniferous forest). Canopy height profiles (CHPs) were estimated from the SLICER waveforms. The indices acquired from the CHPs were: canopy cover, mean canopy height (MCH), maximum height, MCH squared, and mean canopy profile height. The study found that almost every index used was significantly correlated with AGB, with the exception of canopy cover in the temperate deciduous forest. The study found that for the boreal coniferous forest a product of cover as well as several height indices were better predictors than height indices alone. The opposite was found for the temperate deciduous

forest, and at the temperate coniferous forest there was no significant difference between the two sets of variables.

Tsui et al. (2012) performed a study involving multi-frequency radar and discrete-return lidar used for the purpose of estimating AGB and other biomass components. The study was conducted in a temperate forest, located on Vancouver Island, British Columbia, Canada. For the purpose of constructing a predictive model, multiple lidar metrics were calculated and entered into a multiple linear regression analysis. The study found a relatively high correlation between AGB estimation and the lidar metrics of mean first return height and height percentiles (10th and 90th). The study found that a lidar only model functioned significantly better than either of the radar only band models as an estimator of AGB.

A study performed by Zhuang et al. (2015), attempted to estimate AGB by using metrics based on Gaussian decomposition of waveform lidar data. The study took place in three counties in central New York, between the cities of Syracuse and Ithaca. The Gaussian metrics included percentile height metrics, height-weighted metrics, and other Gaussian decomposition-derived metrics. For the purpose of comparison non-Gaussian metrics were also calculated, including: relative height metrics, QMHC, HMRatio, leading edge, and trailing edge. This study found that using Gaussian based waveform metrics resulted in more accurate predictions than using non-Gaussian based metrics. The combined metrics were proven to not be significantly more accurate than using Gaussian metrics alone.

In the study performed by Cao et al. (2014), an attempt was made to use small-footprint discrete return and full-waveform airborne lidar metrics in order to estimate the

total biomass and biomass components in subtropical forests. The study was conducted in Yushan Forest, which is a state-owned national forest park located near Changshu, a town located in Jiangsu province in southeastern China. The discrete return metrics calculated were: selected height measures, percentile height, maximum height, mean height, variability of height measures (such as coefficient of variations in heights), selected canopy return density measures (such as canopy return density), and canopy cover measures (such as canopy cover above 2 m). The full-waveform metrics which were calculated include: height of median energy (HOME), waveform distance (WD), height/median ratio (HTMR), number of peaks (NP), roughness of outermost canopy (ROUGH), front slope angle (FS), return waveform energy (RWE) and vertical distribution ratio (VDR). The study found that discrete return derived metrics were significantly better at predicting AGB than those of the full-waveform. The study also found that by combining the two types of metrics a slightly better predictive model was created, but this model was only slightly more accurate than the discrete return model.

A study by Li et al. (2015) examined the use of small-footprint, discrete-return lidar to estimate the AGB and below-ground biomass (BGB) of maize located in Zhangye City, Gansu Province, China. The metrics calculated for these estimations included maximum height ( $H_{\max}$ ), mean height ( $H_{\text{mean}}$ ), and percentile height ( $H_p$ ), and the laser penetration metric (LPI). The study found a strong correlation between the canopy height and LAI of the maize with the maize's AGB and BGB. Of the lidar metrics  $H_{\max}$  had the strongest correlation to canopy height, explaining 79% of the variance, while the LPI was correlated with LAI, explaining 78% of the variance. The study concluded that the lidar estimates of AGB and BGB were comparable to the field-based measurements,

illustrating that lidar may be useful for estimating canopy height, LAI, and biomass components for maize.

These studies illustrate the feasibility of applying common lidar metrics to SfM point clouds in order to estimate above-ground biomass. Additionally, these studies provide examples of the proper methods and common metrics used for estimating AGB using point clouds.

#### 2.4 Structure from Motion as an alternative to lidar data

More recently, a new technology has emerged as a cost effective alternative to lidar. This technology uses photogrammetric techniques to create a 3D point cloud representation of an area. This technology commonly employs the use of UAVs (Mancini et al. 2013; Mathews and Jensen 2013) in order to obtain the imagery required to produce the point cloud, and thus is not reliant on the expensive cost of hiring a plane or other aerial vehicles to obtain the imagery, nor is it limited by long delays in the return time of satellite imagery (Leberl et al. 2010; White et al. 2013). The technology is also able to implement many algorithms previously developed for lidar data classification, as both are based on point cloud datasets.

In a study undertaken by Snavely et al. (2006) the researchers created a system by which to build 3D models from collections of photographs using SfM developments. This study is an early example of how SfM works, introducing readers to the concepts of image-based modeling, rendering, and SfM with dense point matching. The study explains how 3D models are developed from sets of photographs, a brief history of how this technology was developed, and a demonstration of the technology through the creation of 3D models of historic sites. This study illustrates how SfM is capable of

creating point clouds as well as some of the advantages SfM presents when dealing with imagery.

Leberl et al. (2010) compares the point clouds of lidar vs. those of SfM. The study compared point clouds derived from aerial and street-side lidar systems with those derived from imagery. It was found that in terms of accuracy the SfM point clouds compared well with the lidar point clouds, while vastly surpassing lidar in surface point density. The study also identified 15 other advantages to using SfM over lidar.

In a study performed by White et al. (2013) lidar and SfM point cloud accuracies were compared for the purpose of forest inventories. The study accomplished this by creating DEMs from lidar derived data and digital airborne imagery. The study found that the SfM-based models were as accurate as lidar except for two limitations. The first limitation is that a DEM is required to normalize SfM point clouds' above-ground heights, but due to dense vegetation, high spatial resolution, and vertical accuracy requirements, lidar data may still be required to create the needed DEM in densely vegetated areas. The other identified limitation is that SfM point clouds mainly characterize the outer tree envelopes and do not penetrate the volume under canopy as lidar sensors are capable of due to the ability to penetrate canopy gaps. They concluded that while SfM has limitations, its cost-benefit ratio makes it an ideal technology for much of what is required for forest inventory management.

Fonstad et al. (2013) conducted a study to evaluate the effectiveness of using SfM to create high resolution, high quality DEMs of fluvial topographic environments. The study was conducted on the Pedernales River in Texas and involved acquisition of images through the use of a hand-held helikite. The study compared a lidar-generated

DEM with the SfM-generated DEM and the authors reported that the SfM DEM had better feature representation than the lidar DEM while preserving positional accuracy of the terrain surface. Due to this and the less stringent requirements for data collection the study concludes that SfM presents a genuine alternative to lidar and needs to be researched further.

A study conducted by Mancini et al. (2013) examined the use of SfM for creating high resolution digital surface models (DSMs) for coastal environments. The study utilized a UAV flown at low-altitude to collect the imagery. The point cloud generated from this imagery was compared to one generated by Terrestrial Laser Scanning (TLS) surveys, which is a ground based lidar. DSMs were generated from both systems and the vertical accuracies were assessed. The study found that the SfM method was comparable in terms of accuracy to the TLS method. Because of this level of accuracy and SfM's ease of use the researchers believe that the method is promising and should be further researched.

Since SfM facilitates a cost effective alternative to relatively expensive lidar data and the ability to collect data at almost any time, the technology is becoming increasingly popular and will likely continue to grow in popularity (Dandois et al. 2010; Leberl et al 2010; White et al. 2013). Because of this it is important to continue to investigate what the technology is currently capable of achieving as well as the current limitations that exist when using the technology across various landscapes and cover types.

### III. MATERIALS AND METHODS

#### 3.1 Study area

The study area is located at Freeman Ranch Center (N29° 94' and W97° 99'), located in central Texas northwest of San Marcos, Texas. Freeman Ranch Center is approximately 1,700 hectares in size and lies within the Balconies Canyonlands sub-region of the Eastern Edwards Plateau. The ranch is dominated by *Quercus virginiana* and *Juniperus ashei* trees with the primary family of grass being Poaceae (37 different species present).

The topography is characterized by rugged hills, and shallow valleys as is common in the Edward's Plateau ecoregion. Slopes range from 0 to 14.9 degrees. The soils found on the ranch are often very shallow and exposed bedrock is common (Fowler 2005). There are no long-term weather observations for Freeman Ranch Center, but according to Dixon (2000) the area receives approximately 34 inches of rain annually. The annual temperature range for the study area is 15.5 C°. Summer highs tend to average 32 C° and winter lows tend to average 4.5 C° (Dixon 2000).

The study took place within a pasture that is currently used for grazing and field studies (Figure 1). It is relatively flat and composed primarily of Poaceae grasses. Cacti and trees are also present within or near the study area. The size of the plot used specifically for this study is approximately 0.483 hectares.



**Figure 1.** Study Area. Area where research was conducted.

### 3.2 Field Data

In order to obtain and evaluate the field measurements of true above-ground biomass, a GPS unit with an antenna for improved precision, a 0.5 x 0.5 m grid, a set of clippers, a compass, a drying oven, and a scale were necessary. First, the Trimble GeoXH GeoExplorer 2008 GPS unit attached to a Zephyr antenna on a 2-m range pole was placed at the center of each plot. GPS positions were recorded at a 1 second interval for two to three minutes, resulting in approximately 150 positions that were averaged to create the final feature center point. Next, the 0.5 x 0.5 m grid was placed on the ground with the antenna pole at the center of the grid. The compass was used to align the corners of the grid to NE, SE, SW, and NW so the sides of the grid would be facing the cardinal directions. The antenna was removed from the sampling grid, and all vegetation above 2.5 cm was clipped and stored in plastic trash bags. This process was repeated for each of the 30 plots which were distributed semi-systematically (Figure 2).



**Figure 2.** Location of plots used for collecting AGB.

Once all the AGB samples had been collected and stored, a drying oven and scale were used to properly dry and weigh the AGB. The AGB samples were transferred from the plastic trash bags to brown paper bags in order to help prevent the growth of mold, as well as to fit within the drying oven. Materials from each sample plot were weighed prior to drying and then every day until the weight remained constant, signifying that all water had evaporated from the sample. On average, the drying process took about two days, with the exception of one large sample that took four days. Once the weight of the AGB remained constant, the weight was recorded in grams. The paper bags were weighed and subtracted from the total AGB weight for each plot. All data were recorded into a Microsoft Excel spreadsheet. Field measured AGB served as the dependent variable in the statistical analysis.

### 3.3 Image Acquisition, Processing, and Point Cloud Generation

The imagery for this study were collected using a 3D Robotics X8+ as this UAV system has all the necessary specifications for the collection of imagery needed for SfM to produce a point cloud. All images were obtained a week prior to collection of the AGB data. The image data were collected using multiple transects for the flight paths and from heights ranging from 15 to 25 meters. A GoPro Hero3+ camera was used to acquire imagery at one second intervals. Eight GPS-located ground control points (GCPs) were used in order to georeference the imagery. These GCPs were distributed semi-randomly throughout the study area. Figure 3 shows one of the flight paths as well as the locations of the eight GCPs.



**Figure 3.** Example of a flight path with GCP locations.

Agisoft PhotoScan was used to process the individual images in order to align them and create a mosaic which was then used to perform the dense-point matching. PhotoScan identifies common points within multiple images and through a series of

computations it generates a point cloud. Once these steps were accomplished, the point cloud was exported as a Log ASCII Standard (LAS) file and integrated into ArcMap.

This LAS file was used to create a point-based shape file used for further analysis.

Next, the GPS center points for each of the thirty plots were imported into ArcMap. The plot points were buffered 0.5 m and the feature space to envelope tool used to create polygon shapefiles corresponding to the field plots. The points files derived from the SfM LAS point cloud were clipped to the field plots shape file, so only points that fell within these plots remained. The points within each individual plot were exported as a separate shapefile for each plot.

A 0.5 m<sup>2</sup> lidar-derived inverse distance weighted (IDW) DTM was generated from lidar data obtained from by the Capital Area Council of Governments (CAPCOG) and is available for research purposes at Texas State University. The DTM was created using only returns classified as “ground” in order for the resulting surface model to be used as the ground reference feature. Unfortunately, there was a disagreement in Z values between the lidar-derived IDW and the SfM-derived point shapefile with the lidar DTM possessing Z values that were up to 1.5 m greater than the SfM Z values. To remedy this issue, a technique called Iterative Closest Point (ICP) was used to co-register the lidar and SfM point clouds. ICP has been used by other researchers implementing SfM techniques for vegetation studies (Dandois et al., 2015).

ICP is an algorithm used to align point clouds. Several open source programs can perform ICP, however, this study implemented CloudCompare due to its ease of use and informative tutorials. The algorithm that ICP employs works in the following way: one point cloud, called the reference point cloud, is kept in place while the other point cloud,

the source point cloud, is transformed through a series of iterative passes in order to align it as closely as possible with the reference point cloud. This is accomplished by locating, for each point in the source point cloud, the closest point in the reference point cloud. Then using a mean squared error cost function, the necessary rotation and translation coefficients for each of the source points that best aligns it with the reference points are estimated. Once these estimates are complete, the source point cloud is transformed using the estimates from the previous step. This process is then repeated until the best possible alignment is obtained. In this study, the reference point cloud was the lidar point cloud, while the SfM point cloud was the source.

### 3.4 SfM metric calculations

Predictor covariates (i.e., metrics) were calculated using SfM heights. Heights were calculated by extracting the lidar-based DTM Z values and writing those values to the attribute table in the SfM points shapefile. Then the DTM Z values were subtracted from the referenced SfM points Z values. The resulting values were classified as height and all negative values were excluded from the analysis.

SfM point cloud metrics were calculated from all points with positive height values. Metrics included mean point height ( $h_{\text{mean}}$ ), median height ( $h_{\text{median}}$ ), maximum height ( $h_{\text{max}}$ ), minimum height ( $h_{\text{min}}$ ), 10<sup>th</sup> and 90<sup>th</sup> percentile heights ( $h_{10}$ ,  $h_{90}$ ), percent cover greater than 2.5 cm ( $PC_{2.5}$ ), percent cover greater than 3.5cm ( $PC_{3.5}$ ), percent cover greater than 5 cm ( $PC_5$ ), standard deviation of height ( $h_{SD}$ ), coefficient of variation (CV), and variance (V) (Table 1). These metrics were chosen because they were identified during the literature review as the metrics which were most commonly calculated for predicting AGB through the use of a point cloud. The metrics were calculated in

Microsoft Excel for each plot after exporting the plot attribute tables from ArcMap.

**Table 1.** Summary of Metrics. Summary of the metrics calculated from the SfM point cloud and used as regression covariates to estimate AGB.

<b>Metrics</b>	<b>Description</b>
Mean Height ( $h_{\text{mean}}$ )	The mean height above ground for the SfM points
Median Height ( $h_{\text{median}}$ )	The median height above ground for the SfM points
Maximum Height ( $h_{\text{max}}$ )	The maximum height above ground for the SfM points
Minimum Height ( $h_{\text{min}}$ )	The minimum height above ground for the SfM points
Percentile Heights ( $h_{10}, h_{90}$ )	The percentile height distributions (10th and 90th) for the SfM points
Percent Cover ( $PC_{2.5}, PC_{3.5}, PC_5$ )	The percent of heights located above a certain threshold (2.5 cm, 3.5 cm, 5 cm)
Standard Deviation of Height ( $h_{\text{SD}}$ )	The value of one standard deviation for the SfM points
Coefficient of Variation (CV)	The measurement of dispersion for the SfM points
Variance (V)	The measurement of dispersion from the mean for the SfM points

### 3.5 Statistical Analysis

The calculated metrics, as well as the dried AGB weights were entered into the statistical program JMP Pro 12. The SfM-derived metrics were entered as the independent variables and AGB weight was the dependent variable. The data were analyzed to identify outliers and to ensure a normal distribution in the dependent variable. As plot 8 was a major outlier in terms of its AGB, it was removed from the analysis. Plots 17 and 19 were removed due to being outliers in  $h_{\text{max}}$ ,  $h_{\text{mean}}$ ,  $h_{90}$ , variance, and  $h_{\text{SD}}$  which were a result of unusual artifact features. Plots 16 and 20 through 23 were removed from the analysis as well, due to the lack of positive heights for metric calculation. Since the AGB weights were not normally distributed, their values were transformed using a Log10 transformation.

The all possible models linear regression function was used to identify the model, using up to four covariates at a time, which best predicted AGB. All possible models was selected because it tests every subset of independent variables to identify the best models using all possible combinations of covariates. The output for this analysis was limited to four variables to predict AGB, as it was found during the literature review that most predictive AGB models only used two to four variables. Once the best models were identified, the p-values of the input variables were evaluated to ensure that they were significant at  $\alpha = 0.05$ .

## IV. RESULTS

### 4.1 AGB Field Measurements

AGB weights are presented in Table 2. Plot 8 had the greatest AGB weight of 105.9g after the weight of the storage bags had been subtracted, while plot had the lowest AGB weight of 36g. As illustrated below in Figure 4, the weights are concentrated in the 40 to 70g range.

**Table 2.** Above-ground biomass (AGB) weights by plot.

<b>Plots</b>	<b>Weight with Bags (grams)</b>	<b>AGB Weight (grams)</b>
Plot 1	80.3	60.3
Plot 2	67.5	47.5
Plot 3	56.0	36.0
Plot 4	74.5	54.5
Plot 5	70.5	50.5
Plot 6	149.4	85.6
Plot 7	81.4	61.4
Plot 8	135.9	105.9
Plot 9	78.2	58.2
Plot 10	68.7	48.7
Plot 11	54.0	44.0
Plot 12	63.4	43.4
Plot 13	64.3	54.3
Plot 14	61.2	51.2
Plot 15	63.5	53.5
Plot 16	74.6	54.6
Plot 17	55.2	45.2
Plot 18	46.6	36.6
Plot 19	82.0	62.0
Plot 20	157.6	93.8
Plot 21	84.1	64.1
Plot 22	86.6	76.6
Plot 23	75.5	65.5
Plot 24	59.3	49.3
Plot 25	81.5	71.5
Plot 26	79.3	69.3
Plot 27	68.1	58.1
Plot 28	66.1	56.1
Plot 29	59.7	49.7
Plot 30	61.9	51.9

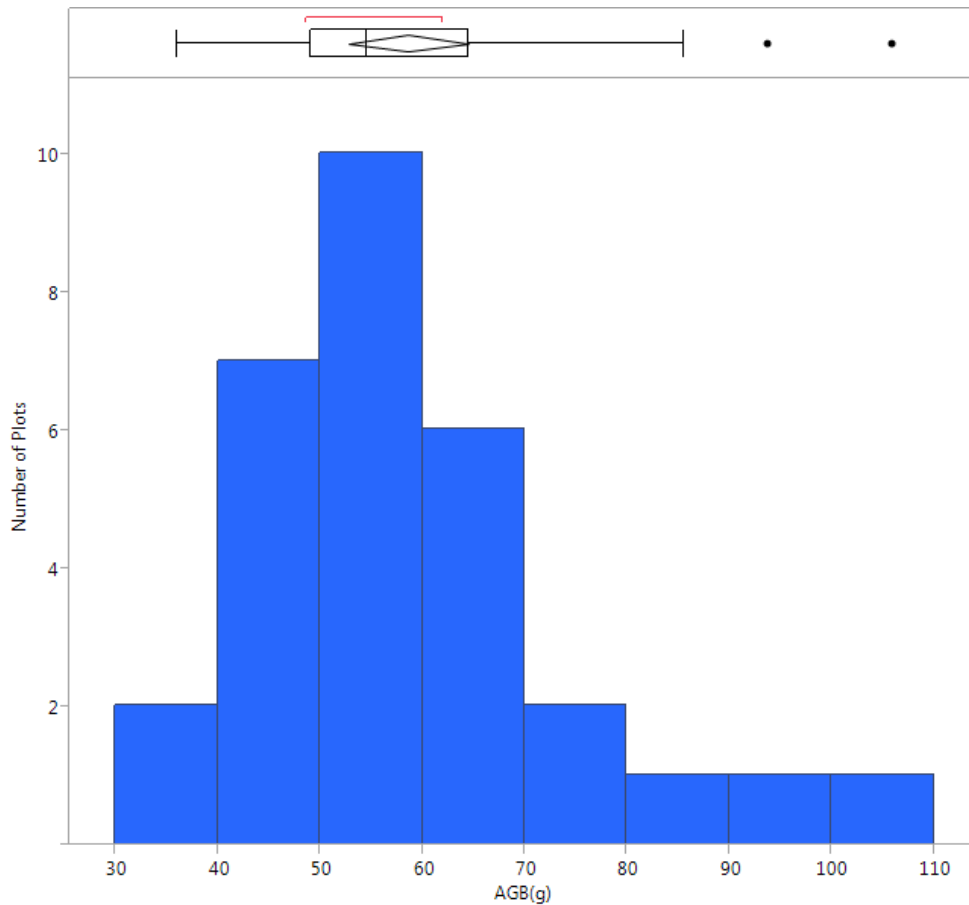


**Figure 4.** Distribution of AGB weights.

As plots 8, 16, 17, 19, 20, 21, 22, and 23 were excluded from the analysis for either lack of data or being clear outliers for either predictor or field-measured variables, the descriptive statistics provided in Table 3 excludes these plots. After excluding these outliers the plot possessing the maximum weight became plot 6, with a weight of 85.6g. This reduces the range of the weights to 49.6g. This also decreased the mean to 54.2g. Interestingly, this still corresponds well with weight distribution illustrated in Figure 2, with the majority of the weights falling between 43g and 65g

**Table 3.** Descriptive statistics of AGB in field-measured plots, excluding outliers.

<b>Statistics</b>	<b>Values (grams)</b>
AGB min	36.0
AGB max	85.6
AGB mean	54.2
AGB standard deviation	11.2
AGB range	49.6

#### 4.2 Results of the SfM and Lidar Point Clouds

Table 4 provides a summary of the data measurements for the SfM and lidar point clouds. The SfM derived point cloud for the entire study area contained a considerably larger number of points than the lidar point cloud, with 7,053,366 total points.

Additionally, given the large number of points, the SfM point cloud had a significantly higher point density and lower nominal point spacing than the lidar derived point cloud. Interestingly, the SfM point cloud corresponding to just the plots that were clipped for analysis had a much lower point density and a higher point spacing.

**Table 4.** SfM and lidar data measurements.

<b>Point Cloud</b>	<b>Number of Points</b>	<b>Point Density</b>	<b>Point Spacing</b>
SfM Study Area Point Cloud	7,053,366	421.1	0.1
SfM Plots Point Cloud	26,187	20.4	0.2
Lidar Point Cloud	5,200,991	2.0	0.7

The distribution of the number of SfM points per plot is displayed in Figure 5. The majority of the plots had 600 to 900 points located within them. Examples of the SfM-derived point cloud for the study area are provided in Figures 6 and 7, while a larger scale example of the plots' point clouds are provided in Figure 8. In these illustrations, elevations are displayed in a range from green to red with low elevations corresponding

to green and high elevations corresponding to red, while the individual plots are displayed in purple.

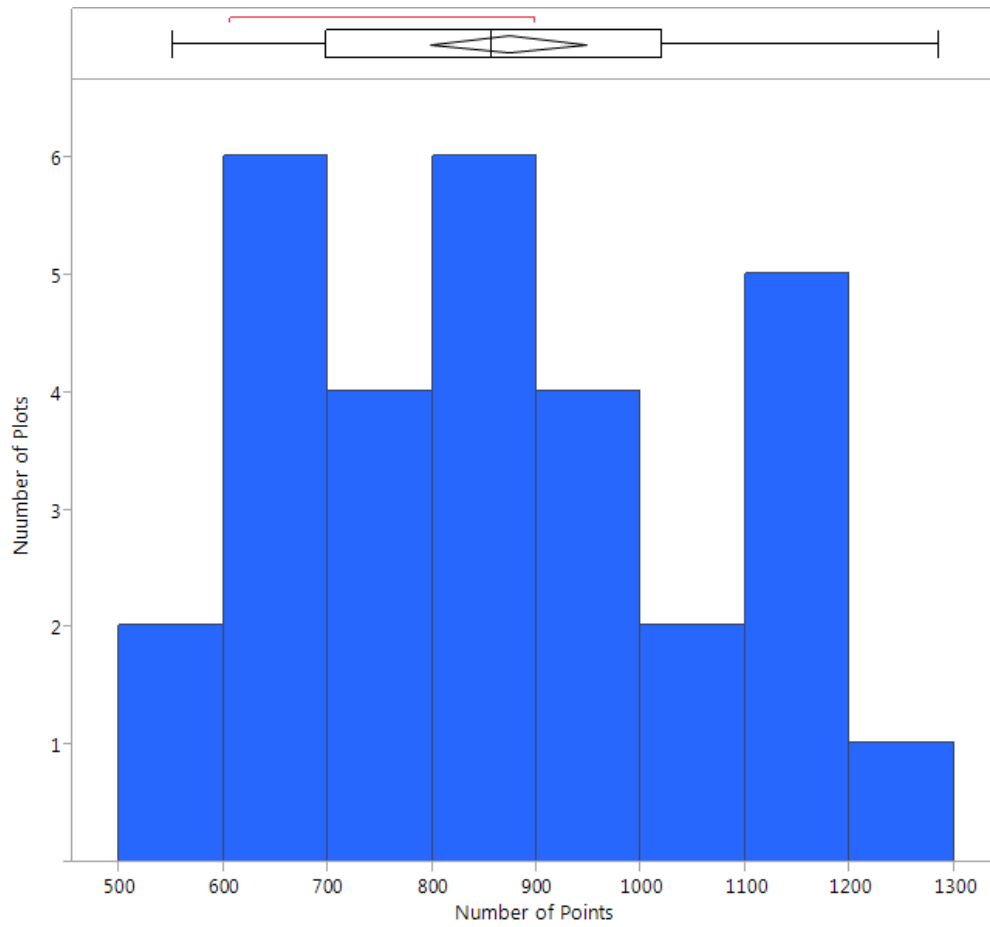


**Figure 5.** Distribution of the number of points per plot.

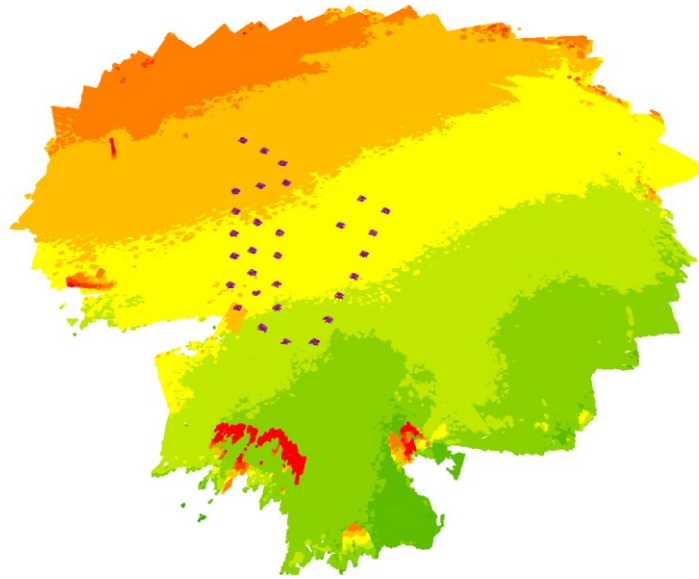


**Figure 6.** Birds-eye view of the study area's SfM point cloud. Elevations are displayed in a range from green to red with low elevations corresponding to green and high elevations corresponding to red, while the individual plots are displayed in purple.

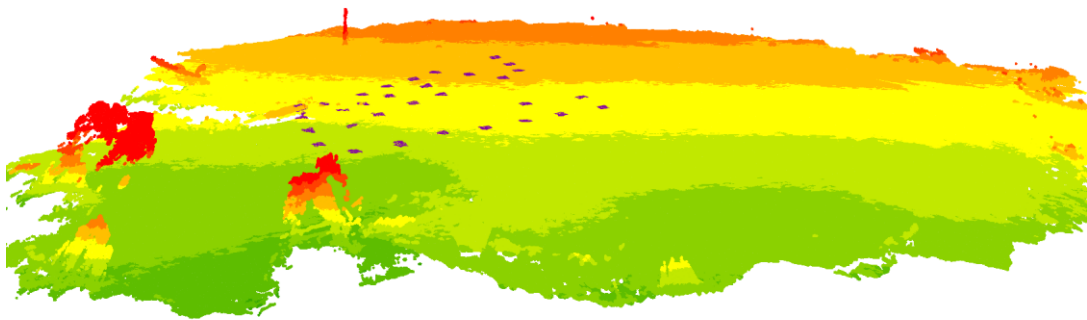


**Figure 7.** Oblique view of the study area's SfM point cloud. Elevations are displayed in a range from green to red with low elevations corresponding to green and high elevations corresponding to red, while the individual plots are displayed in purple.

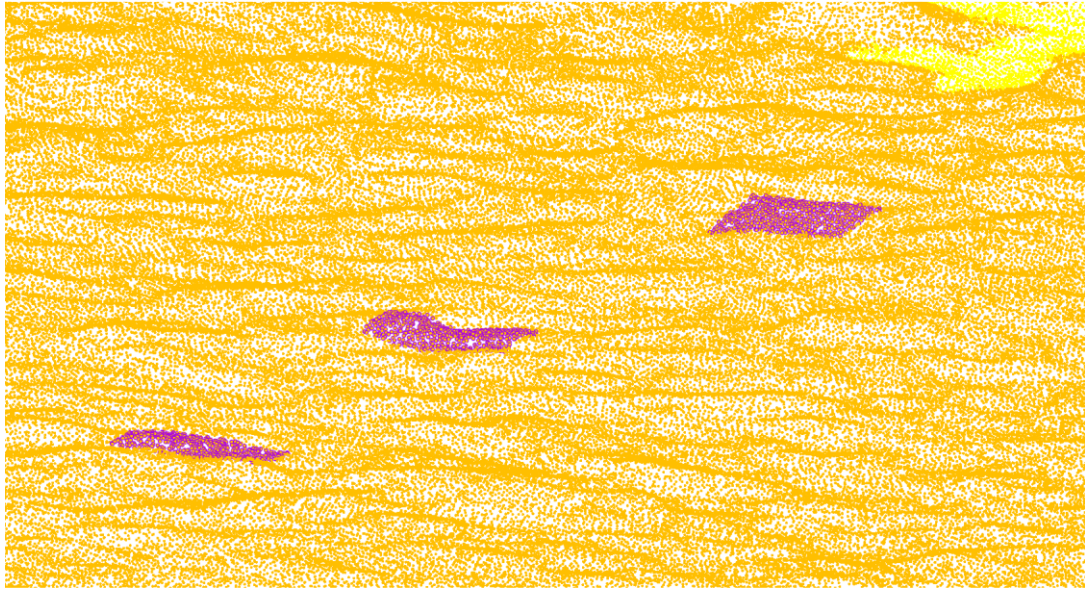


**Figure 8.** Close-up view of the SfM point cloud on plots 1-3.

#### 4.3 Statistical Relationship between SfM Variables and Field Measured AGB

Table 5 presents the descriptive statistics for the SfM-derived metrics used for statistical analysis. The greatest range of values was found in the percent cover above 5cm ( $PC_5$ ) variable, while the lowest range of values was in the variance variable.

**Table 5.** Descriptive statistics of the SfM derived metrics.

<b>Metric</b>	<b>Min</b>	<b>Max</b>	<b>Mean</b>	<b>Standard Deviation</b>	<b>Range</b>
$h_{\text{mean}}$	0.02702	0.22547	0.11845	0.05823	0.19845
$h_{\text{median}}$	0.02300	0.22760	0.11686	0.06123	0.20460
$h_{\text{max}}$	0.09762	0.34926	0.22066	0.07170	0.25164
$h_{\text{min}}$	0.00002	0.13983	0.03378	0.03947	0.13981
$h_{10}$	0.00261	0.18018	0.06932	0.05340	0.17757
$h_{90}$	0.05515	0.27582	0.17012	0.06339	0.22067
$PC_{2.5}$	0.40000	1.00000	0.89747	0.16550	0.60000
$PC_{3.5}$	0.24000	1.00000	0.85373	0.22541	0.76000
$PC_5$	0.15000	1.00000	0.80067	0.28426	0.85000
$h_{\text{sd}}$	0.01932	0.07176	0.03848	0.01138	0.05244
CV	0.15172	0.87606	0.41168	0.21808	0.72434
V	0.00037	0.00515	0.00160	0.00100	0.00478

Goodness-of-fit statistics for individual models are provided in Table 6. Based on the p-values, none of the individual variables were significant for  $\alpha = 0.05$ . Also, as seen in the low  $r^2$  values, none of the variables were robust predictors on their own, with the highest  $r^2$  being 0.121.

**Table 6.** Goodness-of-fit statistics for individual metrics.

<b>Metric</b>	<b><math>r^2</math></b>	<b>Adjusted <math>r^2</math></b>	<b>RMSE</b>	<b>p-value</b>
$h_{\text{mean}}$	0.10519	0.06045	0.08445	0.1409
$h_{\text{median}}$	0.09286	0.04751	0.08503	0.1679
$h_{\text{max}}$	0.088	0.043243	0.08522	0.178
$h_{\text{min}}$	0.10964	0.06512	0.08424	0.1323
$h_{10}$	0.08991	0.04441	0.08517	0.1752
$h_{90}$	0.12143	0.0775	0.08368	0.112
PC <sub>2.5</sub>	0.00069	-0.04937	0.08925	0.9075
PC <sub>3.5</sub>	0.00049	-0.04949	0.08926	0.9225
PC <sub>5</sub>	0.00041	-0.04957	0.08926	0.9291
$h_{\text{sd}}$	0.048924	0.00137	0.08707	0.3226
CV	0.00241	-0.04747	0.08917	0.8283
V	0.04516	-0.00258	0.08724	0.3424

Table 7 provides statistical summaries of the four models generated by the all possible models method. Validation was accomplished by using the predicted residual error sum of squares (PRESS) statistic. Unfortunately, none of the models achieved a high  $R^2$ , though the 4 covariate model was able to explain 36 percent of the variation in field measured AGB values. Interestingly, the only model that was significant at  $\alpha = 0.05$  was the 2 covariate model, which used  $h_{90}$  and PC<sub>5</sub> to predict AGB. A scatterplot with a regression line for the 2 covariate model is presented in Figure 9.

**Table 7.** Summary of model statistics.

Model	Covariates	R <sup>2</sup>	Adjusted R <sup>2</sup>	RMSE	F Ratio	p-value	PRESS
1Covariate	$h_{90}$	0.12	0.08	0.08	2.76	0.11	1.02
2Covariates	$h_{90}, PC_5$	0.31	0.24	0.08	4.24	0.03	0.96
3Covariates	$h_{mean}, h_{max}, CV$	0.34	0.23	0.08	3.13	0.05	0.96
4Covariates	$h_{min}, h_{90}, PC_{3.5}, PC_5$	0.36	0.21	0.08	2.41	0.09	1.01

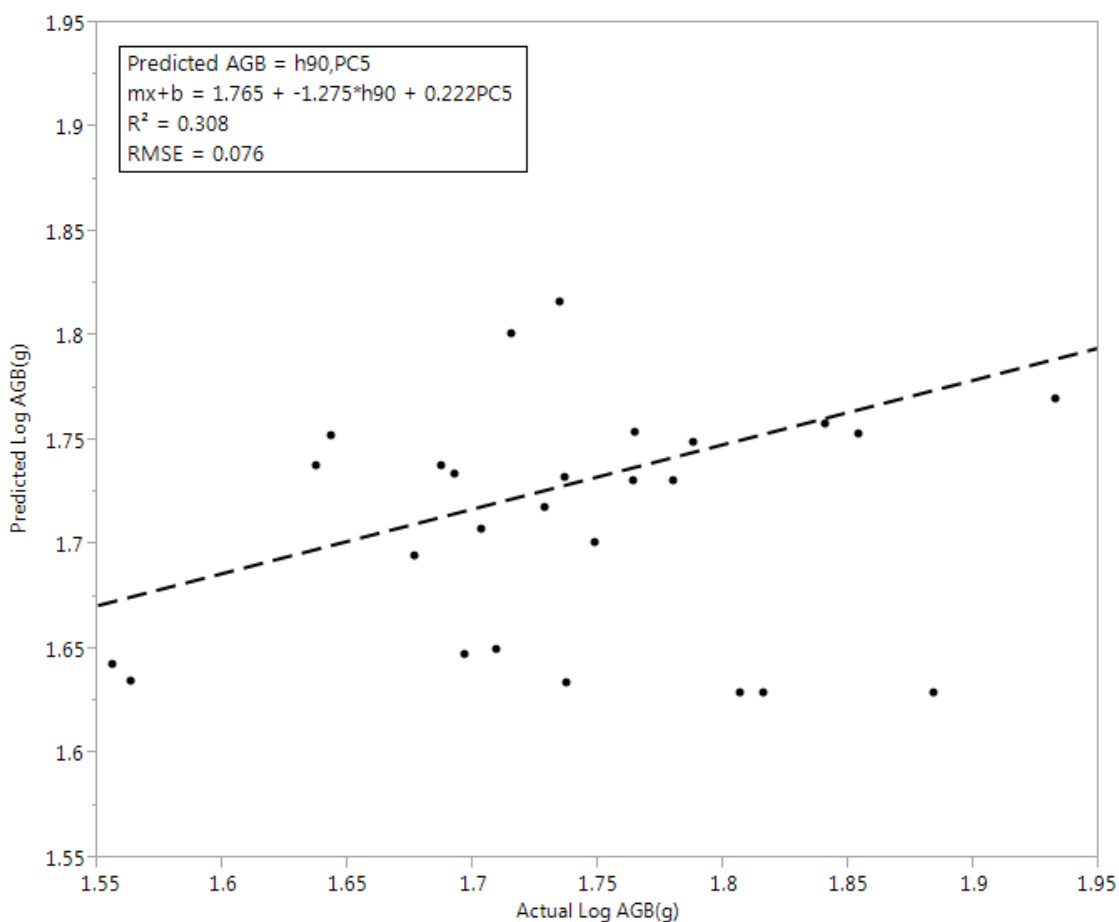


**Figure 9.** Two SfM covariate multiple regression model of actual versus predicted AGB.

## V. DISCUSSION

### 5.1 SfM prediction of AGB

Based on the results, the SfM-derived point cloud proved to be a poor predictor of AGB for the pasture located at Freeman Ranch Center. The 2 covariate model was the only model that was significant for  $\alpha = 0.05$ . Despite overall model significance, the  $R^2$  of 0.31 demonstrates that the model could only account for 31 percent of the variability in field-measured AGB among the 22 plots used for analysis.

The three remaining models were not statistically significant. Of these remaining three models, only the 3 and 4 covariate models possessed a higher  $R^2$  than the 2 covariates model, with  $R^2$  values of 0.34 and 0.36, respectively. This increase in explained variance is rendered inconsequential due to the lack of statistical significance. Also, the addition of too many covariates can lead to multicollinearity, which could be legitimate in this study as many of the predictor variables were based on height and were highly correlated.

He et al. (2013) found that lidar was able to predict the AGB of a coniferous forest through the use of height and percent cover metrics. The mean height and crown cover were the best predictors of AGB, resulting in an  $R^2$  of 0.74. The research outlined in this paper attempted a similar study using SfM in a pasture environment, but could not achieve similar accuracies to their study. Other lidar studies have also proved successful at estimating AGB with height based metrics (Lefsky et al., 2002; Drake et al., 2003; Kankare et al., 2013; Cao et al., 2014). Li et al.'s (2015) study found that canopy height and LAI best predicted maize crop AGB, with an  $R^2$  of 0.87. This study illustrates that metrics used in lidar forest studies were successfully implemented in maize croplands.

While these two studies examined different environments, they both achieved robust predictive models based on similar metrics. I hypothesized that using similar metrics would result in a similar model for AGB estimates in pasture environments.

Leberl et al. (2010) and White et al. (2013) both found that lidar and SfM point clouds were comparable in accuracy. This research does not contradict this entirely, but when compared to the accuracy of AGB estimations in other studies it did fail to produce similar results. Additionally, there was a large discrepancy between the SfM Z values and those of the lidar data.

The inability of the SfM point cloud metrics to predict AGB of a pasture environment could be the result of many potential inconsistencies and limitations. The remainder of this chapter will examine the inconsistencies between the SfM and lidar point clouds, uncertainties and limitations of the SfM method, and ways to potentially improve the predictive model for future research.

## 5.2 SfM and Lidar Inconsistencies

Inconsistencies between the lidar and SfM point clouds heights were discovered early on in the study, when heights were calculated using the lidar-DTM and the SfM point cloud. The majority of the SfM points were located about 1.5 m below the lidar generated DTM, which resulted in negative height values for SfM metric calculation. In order to ensure that this was not caused by an error during the generation of the SfM points, the GPS control points and plot center point Z values were compared directly with the lidar Z values.

A number of steps were taken to identify the cause of the discrepancy and remedy the error. First, all of the GPS data was again re-exported and compared to the lidar data.

As the error still persisted, the GPS unit was taken back to the field site and plot center point coordinates were reacquired as close to the original GPS points as possible. The data were processed and compared to the lidar data, but the error remained. The lidar data were examined to determine if the scan angle, during acquisition over the study area, were within  $\pm 15$  degrees from nadir, as this is the commonly accepted range for vegetation characterization (McGaughey et al., 2006; Nayegandhi, 2007). Unfortunately, the lidar data attributes omitted scan angles. This analysis resulted in the discovery that the lidar ground data elevations may have been incorrect.

Because I was unable to identify the exact cause of the discrepancy in Z values, the ICP algorithm was used to shift the SfM data to match the lidar data. The ICP algorithm matched the SfM point cloud to the lidar point cloud. However, certain plots in the SfM point cloud still lacked any positive height values, though the majority of the plots exhibited all positive heights. One reason that negative heights may have still existed even after the application of the ICP method is the lidar pulses did not actually penetrate the dense standing grass. This would lead to these points being identified as ground returns even though they could be up to a meter above the actual ground. Hodgson et al. (2003) noted the difficulty of differentiating ground returns from low lying shrubs/shrubbery, stating that errors of up to 112 cm can occur as a result. Pelletier et al. (2011) found that areas consisting of thick grasses may be falsely identified as ground returns resulting in an error of a meter or greater. These studies support the hypothesis that the lidar pulses in this area may have been falsely classified as ground when in fact they were vegetation.

Another inconsistency between the lidar derived point cloud and the SfM point

cloud was the point density. The SfM point cloud had a considerably higher point density on both the study area scale as well as for the individual plot level. The lidar data's average point spacing was much higher than the SfM's. This should not be an issue because the average point density was greater than the 0.06 point per meter squared threshold and lidar data with point densities above this threshold are considered acceptable for building some of the highest level resolution DEMs (Anderson, 2009; Sanii, 2008). In a study by Anderson (2009) it was found that in order to produce accurate DEMs at least 60,000 points per square kilometer are needed (0.06 per square meter). Sanii (2008) found that once point density falls below 0.06 the RMSE for elevation goes from increasing linearly to exponentially. The point density of the lidar for this research was 2 points per square meter.

While a discrepancy in point density and spacing existed, it was expected going into the study as SfM point clouds have been shown to have higher point densities than their lidar counterparts (Leberl et al., 2010; White et al., 2013; Fonstad et al., 2013; Jensen and Mathews, 2016). The height discrepancy still existed in five plots, but the remainder of the plots contained numerous positive point heights, while before there were no positive heights. The potential causes for these inconsistencies were still unclear and required further examination.

### 5.3 Causes of Uncertainty and Limitations to the SfM Method

One possible cause for the uncertainty between the lidar and SfM data could have been that the lidar points in this area had exceeded the acceptable scan angle range. This could have led to the lidar Z values being greater than what they should have been. It has been found that lidar scan angles exceeding certain thresholds can cause errors in Z

values (Holmgren et al., 2003; Sue et al., 2006; Ahokas, 2013). This is unlikely due to these lidar data being accurate in other parts of the general study area. The only reason this may have occurred is the acceptable scan angle for topographic mapping is  $\pm 20$ -30 degrees (McGaughey et al., 2006). According to the CAPCOG data collection report the maximum possible scan angle was 36 degrees for one of the data collection flights and 40 degrees for the other. Both of these scan angles exceed the maximum scan angle recommended by Sue et al. (2006), McGaughey et al. (2006), and the USGS (Nayegandhi, 2007). Because the scan angles are not included in the point attributes the possibility that the points used for this study exceeded an acceptable scanning angle cannot be completely ruled out.

A second cause for error could be that the GPS data obtained erroneous Z values, leading to lower SfM heights than what actually existed. These erroneous Z values are the foundation for the SfM point cloud's heights so this issue would affect all subsequent steps. However, erroneous Z values collected by the GPS unit seems unlikely as the GPS data's accuracy was 0.1m and the X and Y coordinates were accurate. Additionally, all proper procedures for ensuring quality GPS data were followed, including letting the GPS unit acquire a satellite lock and maintain the lock for at least fifteen minutes, ensuring a low PDOP value (i.e.,  $PDOP \leq 3.0$ ), enforcing satellite-based augmentation system (SBAS) real-time corrections, and setting accuracy thresholds data collection (i.e., estimated post-processing accuracy  $\leq 10$ cm).

Limitations of the SfM method derive mainly from the imagery used to create the point cloud. As SfM points are generated by conjugate pixel pairs across multiple images, image blurring could have contributed to errors in the identification of points. This could

lead to some vegetation being left out of the point cloud entirely, or identified at a false height. Jensen and Mathews (2016) found that blurred images used in the generation of a SfM point cloud can cause points to be located significantly above or below the actual position of the feature. Dandois and Ellis (2013) found that there are many factors, such as lighting, wind, vegetation type, etc., that may affect the feature identification and matching algorithms causing inconsistencies in the SfM point cloud. If this occurred frequently, then the plot heights would not accurately represent the vegetation surface. This would lead to an inaccurate model as the height metrics would not truly represent the vegetation within the plots.

The perimeter edges of the SfM point cloud ended up warped, with points being placed in higher elevations than where they would be otherwise (Figures 10 and 11). The issues associated with blurring may be the cause of the warping of the perimeter. This warping causes inaccuracies in height calculations along edge areas, making them unusable for accurate predictive models. It is for this reason that plots 17 and 19 were identified as outliers. As seen in Figure 11, both plots had been distorted due to their proximity to a warped edge.

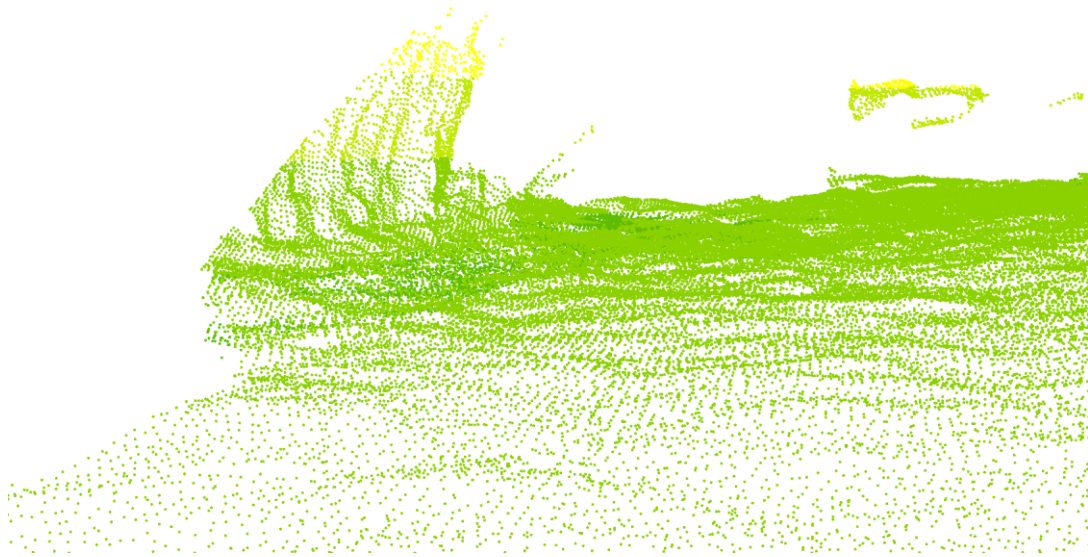


**Figure 10.** Example of a warped edge in the SfM point cloud. Elevation is represented by the color of the pixels, with low elevations being green and higher elevations being yellow.

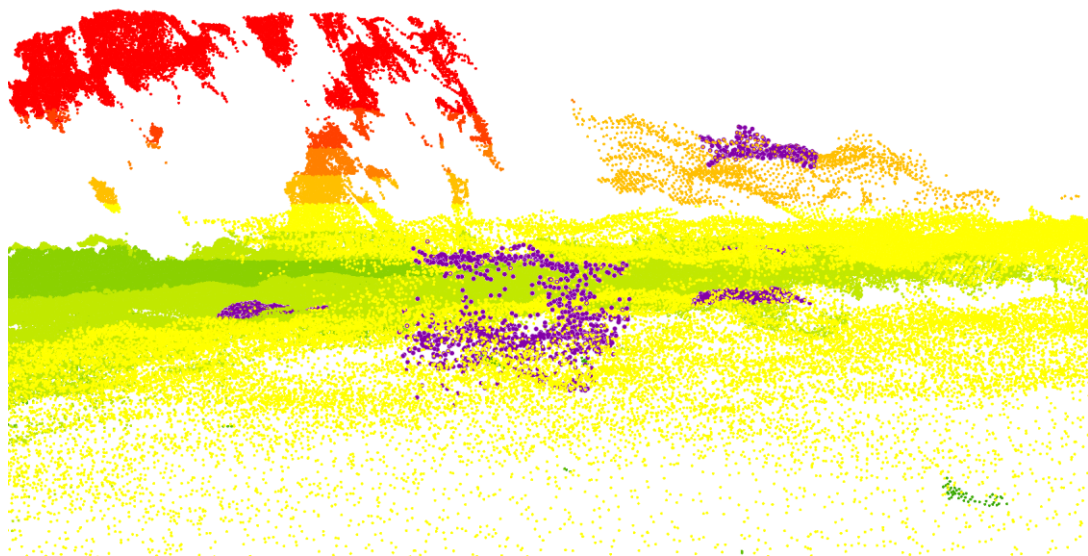


**Figure 11.** Example of two plots affected by warping along the edges. Plot 17 is displayed as purple points in the center of the figure, and plot 19 is displayed with purple points positioned high above the actual surface on the right of the figure. The elevation is displayed through the pixels with colors ranging from green to red. Green pixels represent the lowest elevations while red represent the highest

#### 5.4 Potential Improvements

The image acquisition could have been improved by increasing the number of overlapping flights. This would have increased the number of images and camera perspectives of ground features. With more overlapping flights the heights of the flights could have contained greater variation. The flights in this study ranged from 15 to 25 meters. By adjusting these heights to 10 to 25 meters it is possible that the SfM algorithms would be able to better identify individual grasses as the program would have multiple perspectives of the same feature. Additionally, by increasing the area that obtained imagery for the SfM point cloud the warped edges would have been moved further from the field data collection area. As this warping affected plots 19 and 17, a larger image acquisition area would have resolved this issue, which would have allowed these plots to be included in the model generation.

Before ever acquiring images the GPS data should be checked against the lidar DTM to ensure that Z values are in agreement. ICP has been shown to be an effective method for registering SfM point clouds (Dandois et al., 2015; Yang & Chen, 2015; Marani et al., 2016), but the fact that there was such a tremendous disagreement between the GPS and lidar Z values is still a cause for concern.

It is important to determine if the lidar pulses classified as ground returns actually penetrated the dense grasses. As the lidar data were collected nearly a decade prior to the study, the condition of the vegetation in the study area at the time of collection is difficult to determine. An updated lidar collection with known vegetation conditions, field samples, and corresponding GPS collection would allow for this issue to be addressed. If it was determined that the lidar pulses were reflected off the grasses and shrubbery but

still classified as ground returns then that would indicate that predicting AGB in this pasture using SfM would be difficult. If the lidar returns did truly indicate the bare earth surface to an acceptable degree, then further research into using SfM to estimating the AGB for this pasture would be more conceivable. Unfortunately, the process of studying this issue is beyond the scope of this research.

The method used for statistical analysis may not be appropriate for these data in this environment. Regression trees offer an alternative statistical analysis approach. Regression trees involves using each of the independent variables to fit the regression model. Then each independent variable is split at different split points. The error at each split point is squared to obtain the sum of squared errors (SSE). The split points are then compared and points possessing the lowest SSE are chosen as predictors. This method is considered an effective alternative to multivariate regression (De'ath & Fabricius, 2000; Lawrence & Wright, 2001), and has been used successfully in multiple lidar studies (Falkowski et al., 2009; Pittman et al., 2009; Latifi et al., 2010; Im et al., 2011).

An alternative method for AGB prediction in pastures that has proven effective is spectral analysis. Multiple studies have accurately predicted AGB in grasslands using space-borne sensors such as Landsat (Ullah et al. 2012; Barrachina et al., 2014; Porter et al. 2014; Raval et al. 2014). Spectral analysis used for estimating AGB involves the use of vegetation indices like NDVI and EVI. As the SfM method involves the collection of hundreds of images that can be mosaicked into an orthophoto it should be possible to perform a spectral analysis on this area at a higher spatial resolution than can be obtained from most space-borne sensors.

Another alternative for estimating AGB of a pasture environment is a

combination of point cloud derived metrics with spectral analysis metrics. Using this method allows for the use of spectral analysis metrics in addition to the point cloud metrics. There have been multiple successful studies which have combined lidar and imagery (Rottensteiner et al., 2005; Sohn & Dowman, 2007; Dalponte et al., 2008; Erdody & Moskal, 2009; Sankey & Glenn, 2011). A study which used lidar and multispectral data to estimate plot-level volume and biomass for deciduous and pine forest was performed by Popescu et al. (2004), and it concluded that the use of imagery combined with lidar was always better at predicting volume and biomass than using lidar by itself. Due to the enhancements in predictability by combining lidar data with imagery, it is possible that SfM derived point clouds data combined with imagery would generate a better predictive model for estimating pasture AGB.

## VI. CONCLUSION

This study attempted to estimate AGB of a pasture environment using SfM. Pastures play a crucial role in the environment and AGB is one of the most important characteristics that can be measured in any environment. The imagery was obtained through multiple drone flights using a GoPro Hero 3+ and compiled into a point cloud which was used to calculate predictor metrics. All-possible-models was used to determine the best model for predicting AGB. Unfortunately, none of the models accurately predicted AGB, with the only significant model possessing an  $R^2$  of 0.31. As such, I report that SfM could not accurately estimate AGB in the pasture environment measured at Freeman Ranch Center. Future research should be conducted into alternative methods of collecting and/or analyzing SfM data for estimating AGB in pasture environments.

## LITERATURE CITED

- Anderson B. 2008. Assessing accuracy in varying LIDAR data point densities in digital elevation maps, Master's Thesis, Naval Postgraduate School, Monterey, California.
- Ahokas E. 2013. Aspects of accuracy, scanning angle optimization, and intensity calibration related to nationwide laser scanning, Doctoral Thesis, Publications of the Finnish Geodetic Institute.
- Barrachina M, Cristobal, Tulla A.F. 2014. Estimating above-ground biomass on mountain meadows and pastures through remote sensing. *International Journal of Applied Earth Observation and Geoinformation*. 38: 184-192.
- Cao L, Coops N, Innes J, Dai J, She G. 2014. Mapping Above- and Below-Ground Biomass Components in Subtropical Forests Using Small-Footprint LiDAR. *Forest*. 5: 1356-1373.
- Dalponte M, Bruzzone L, Gianelle D. 2008. Fusion of hyperspectral and LIDAR remote sensing data for classification of complex forest areas. *IEEE Transactions on Geoscience and Remote Sensing*. 46(5): 1416-1427.
- Dandois J, Ellis E. 2010. Remote Sensing of Vegetation Structure Using Computer Vision. *Remote Sensing*. 2: 1157-1176.
- Dandois, J, Ellis, E. 2013. High spatial resolution three-dimensional mapping of vegetation spectral dynamics using computer vision. *Remote Sensing of Environment*. 136: 259-276.
- Dandois J, Olano M, Ellis E. 2015. Optimal Altitude, Overlap, and Weather Conditions for Computer Vision UAV Estimates of Forest Structure. *Remote Sensing* 7(10): 13895-13920.
- De'ath G, Fabricius K. 2000. Classification and regression trees: a powerful yet simple technique for ecological data analysis. *Ecology*. 81(11): 3178-3192.
- Dixon R. 2000. Climatology of the Freeman Ranch, Hays County, Texas. *Freeman Ranch Publication Series*. 3: 2000.
- Drake J, Knox R, Dubayah R, Clark D, Condit R, Blair J, Hofton M. 2003. Above-ground biomass estimation in closed Neotropical forests using lidar remote sensing: factors affecting the generality of relationships. *Global Ecology & Biogeography*. 12: 147-159.
- Erdody T, Moskal L. 2010. Fusion of LiDAR and imagery for estimating forest canopy fuels. *Remote Sensing of Environment*. 114(4): 725-737.

- Falkowski M, Evans J, Martinuzzi S, Gessler P, Hudak A. 2009. Characterizing forest succession with lidar data: An evaluation for the Inland Northwest, USA. *Remote Sensing of Environment*. 113(5): 946-956.
- Fowler N. 2005. An Introduction to the Vegetation and Ecology of the Eastern Edwards Plateau (Hill Country) of Texas. *Edward's Plateau Ecology*: 1-16.
- Fonstad M, Dietrich J, Courville B, Jensen J, Carbonneau P. 2013. Topographic structure from motion: a new development in photogrammetric measurement. *Earth Surface Processes and Landforms*. 38: 421-430.
- Gao J, Chen Y, Lu S, Feng C, Chang X, Ye S, Liu J. 2012. A ground spectral model for estimating biomass at the peak of the growing season in Hulunbeier grassland, Inner Mongolia, Chian. *International Journal of Remote Sensing*. 33(13): 44029-4043.
- Gitelson A, Vina A, Arkebauer T, Rundquist D, Keydan G, Leavitt B. 2003. Remote estimation of leaf area index and green leaf biomass in maize canopies. *Geophysical Research Letters*. 30(5).
- He Q, Chen E, An R, Li Y. 2013. Above-Ground Biomass and Biomass Components Estimation Using Lidar Data in a Coniferous Forest. *Forests*. 4: 984-1002.
- Hodgson, M. E., Jensen, J. R., Schmidt, L., Schill, S., & Davis, B. (2003). An evaluation of LIDAR-and IFSAR-derived digital elevation models in leaf-on conditions with USGS Level 1 and Level 2 DEMs. *Remote Sensing of Environment*. 84(2), 295-308.
- Im J, Lu Z, Rhee J, Quackenbush L. 2012. Impervious surface quantification using a synthesis of artificial immune networks and decision/regression trees from multi-sensor data. *Remote Sensing of Environment*. 117: 102-113.
- Jensen, J, Mathews, A. 2016. Assessment of Image-Based Point Cloud Products to Generate a Bare Earth Surface and Estimate Canopy Heights in a Woodland Ecosystem. *Remote Sensing*. 8(1): 50.
- Jin Y, Yang X, Qiu J, Li J, Gao T, Wu Q, Zhao F, Ma H, Yu H, Xu B. Remote Sensing-Based Biomass Estimation and Its Spatio-Temporal Variations in Temperate Grassland, Northern China. *Remote Sensing*. 6: 1469-1513.
- Kaasalainen S, Holopainen M, Karjalainen M, Vastaranta M, Kankare V, Karila K, Osanoglu B. 2015. Combining Lidar and Synthetic Aperture Radar Data to Estimate Forest Biomass: Stats and Prospects. *Forests*. 6: 252-270.
- Kaiser A, Neugirg F, Rock G, Müller C, Haas F, Ries J, Schmidt J. 2014. Small-Scale Surface Reconstruction and Volume Calculation of Soil Erosion in Complex Moroccan Gully Morphology Using Structure from Motion. *Remote Sensing*. 6: 7050-7080.

- Kankare V, Vastaranta M, Holopainen M, Rätty M, Yu, X., Hyyppä J, Hyyppä H, Alho P, Viitala R. 2013. Retrieval of forest aboveground biomass and stem volume with airborne scanning LiDAR. *Remote Sensing*. 5(5): 2257-2274.
- Latifi H, Nothdurft A, Koch B. 2010. Non-parametric prediction and mapping of standing timber volume and biomass in a temperate forest: application of multiple optical/LiDAR-derived predictors. *Forestry*. 83(4): 395-407.
- Lawrence R, Wright A. 2001. Rule-based classification systems using classification and regression tree (CART) analysis. *Photogrammetric engineering and remote sensing*. 67(10): 1137-1142.
- Leberl F, Irschara A, Pock T, Meixner P, Gruber M, Scholz S, Wiechert A. 2010. Point Clouds: Lidar versus 3D Vision. *Photogrammetric Engineering & Remote Sensing*. 76(10): 1123-1134.
- Lefsky M, Cohen W, Harding D, Parker G, Acker S, Gower S. 2002. Lidar remote sensing of above-ground biomass in three biomes. *Global Ecology & Biogeography*. 11: 393-399.
- Li W, Niu Z, Huang N, Wang C, Gao S, Wu C. 2015. Airborne LiDAR technique for estimating biomass components of maize: A case study in Zhangye City, Northwest China. *Ecological Indicators*. 57: 486-496.
- Lu D. 2005. Aboveground biomass estimation using Landsat TM data in the Brazilian Amazon. *International Journal of Remote Sensing*. 26(12): 2509-2525.
- Mancini F, Dubbini M, Gattelli M, Stecchi F, Fabbri S, Gabbianelli G. 2013. Using Unmanned Aerial Vehicles (UAV) for High-Resolution Reconstruction of Topography: The Structure from Motion Approach on Coastal Environments. *Remote Sensing*. 5: 6880-6898.
- Marani R, Renò V, Nitti M, D'Orazio T, Stella E. 2016. A Modified Iterative Closest Point Algorithm for 3D Point Cloud Registration. *Computer-Aided Civil and Infrastructure Engineering*. 31(7): 515-534.
- Mathews A, Jensen J. 2013. Visualizing and Quantifying Vineyard Canopy LAI Using Unmanned Aerial Vehicle (UAV) Collected High Density Structure from Motion Point Cloud. *Remote Sensing*. 5: 2164-2183.
- McGaughey R.J, Andersen H.E, and Reutebuch, S.E. 2006. Considerations for planning, acquiring, and processing LiDAR data for forestry applications. In Proceedings of the 11<sup>th</sup> Biennial USDA Forest Service Remote Sensing Applications Conference, April 24-28 2006, Salt Lake City, USA.
- Pelletier J, Swetnam T, Papuga S, Nelson K, Brooks P, Harpold, A.A., Chorover, J. 2011. Distinguishing grass from ground using LiDAR: Techniques and applications. AGU Fall Meeting Presentations Abstract EP51E-05.

- Pittman S, Costa B, Battista, T. 2009. Using lidar bathymetry and boosted regression trees to predict the diversity and abundance of fish and corals. *Journal of Coastal Research*. 53: 27-38.
- Popescu S, Wynne R, Scrivani, J. 2004. Fusion of small-footprint lidar and multispectral data to estimate plot-level volume and biomass in deciduous and pine forests in Virginia, USA. *Forest Science*. 50(4): 551-565.
- Porter T, Chen C, Long J, Lawrence R, Sowell B. 2014. Estimating biomass on CPR pastureland: A comparison of remote sensing techniques. *Biomass and Bioenergy*. 66: 268-274.
- Raval S, Sarver E, Shamsoddini A, Zipper C, Donovan P, Evans D, Chu H.T. 2014. Satellite remote sensing-based estimations of biomass production on reclaimed coal mines. *Mining Engineering*. 66(4): 76-82.
- Richter R, Behrens M, Döllner J. 2013. Object class segmentation of massive 3D point clouds of urban areas using point cloud topology. *International Journal of remote Sensing*. 34 (23): 8408-8424.
- Rottensteiner F, Trinder J, Clode S, Kubik K. 2005. Using the Dempster–Shafer method for the fusion of LIDAR data and multi-spectral images for building detection. *Information fusion*. 6(4): 283-300.
- Sanii, S. 2008. Assessing the effect of point density and terrain complexity on the quality of LiDAR-derived DEMs in multiple resolutions. Master on Geographic Information Systems, University of Calgary, Alberta, Canada.
- Sankey T, & Glenn N. 2011. Landsat-5 TM and lidar fusion for sub-pixel juniper tree cover estimates in a western rangeland. *Photogrammetric Engineering & Remote Sensing*. 77(12): 1241-1248.
- Sohn G, Dowman I. 2007. Data fusion of high-resolution satellite imagery and LiDAR data for automatic building extraction. *ISPRS Journal of Photogrammetry and Remote Sensing*. 62(1): 43-63.
- Snavely N, Seitz S, Szeliski R. 2006. Photo Tourism: Exploring Photo Collections in 3D. *ACM Transactions on Graphics*. 25(3): 835-846.
- Su J, Edward B. 2006. Influence of vegetation, slope, and lidar sampling angle on DEM accuracy. *Photogrammetric Engineering & Remote Sensing* 72.11: 1265-1274.
- Tsui O, Coops N, Wulder M, Marshall P, McCradle A. 2012. Using multi-frequency radar and discrete-return LiDAR measurements to estimate above-ground biomass and biomass components in a coastal temperate forest. *ISPRS Journal of Photogrammetry and Remote Sensing*. 69: 121-133.

- Ullah S, Si Y, Schlerf M, Skidmore A, Shafique M, Iqbal I. 2012. Estimation of grassland biomass and nitrogen using MERIS data. *International Journal of Applied Earth Observation and Geoinformation*. 19: 196-204.
- Nayegandhi A. 2007. Lidar Technology Overview. USGS Airborne Lidar Technology and Applications, June 20-21 2007, Baton Rouge, LA.
- Yang B, Chen C. 2015. Automatic registration of UAV-borne sequent images and LiDAR data. *ISPRS Journal of Photogrammetry and Remote Sensing*. 101: 262-274.